1.4 CONNECTIONS BETWEEN PV INTRUSIONS AND TROPICAL CONVECTION

Beatriz M. Funatsu* and Darryn Waugh
The Johns Hopkins University, Baltimore, MD

1. INTRODUCTION

Stratospheric intrusions into the tropical upper troposphere occur in regions of westerly winds within the equatorial easterlies belt. In the central and eastern Pacific in the Northern Hemisphere such disturbances are linked to the development of convection (e.g., Kiladis and Weickmann 1992, Kiladis 1998, Waugh and Funatsu 2003). It has been suggested that the convection occurs in the upward motion induced by the advection of positive vorticity ahead of the trough axis (e.g., Kiladis 1998). We investigate these using version 3 of the Penn State / NCAR MM5 mesoscale model (Grell et al, 1994). Two main questions are addressed: (1) What is the role of the PV in producing favorable conditions for convection?, and (2) What is the impact of latent heat release on the evolution of the PV? Here we show results from simulations of an intrusion event that occurred between 13-17 of January 1987.

2. MODEL

The MM5 simulations presented below used a single domain covering the region 0-44°N and 180-254°W, with horizontal resolution of 50km. The model top is set at 50hP and 31 unevenly spaced σ-levels are used, with slightly higher resolution in the upper troposphere and the boundary layer.

NCEP reanalysis data are used for initial and boundary conditions. In the simulations presented the geopotential and horizontal wind fields are replaced by balanced fields obtained by PV inversion using Davis and Emanuel (1991) technique. We use balanced fields to initialize the runs because it allows for a balanced dynamical field without spurious waves even when the upper level PV is removed, and therefore, results will be self-consistent and comparison between different runs will be meaningful.

**Corresponding author address*: Beatriz M. Funatsu, The Johns Hopkins University, Dept. of Earth and Planetary Sci., 3400 N Charles St., Baltimore, MD 21218;
Email: beatriz@rua.eps.jhu.edu.

3. SENSITIVITY ANALYSIS

We conducted a series of simulations using the setup described in the previous section. In all, the initial condition was set on 13 of January 1987 00UTC (hereinafter we will refer to dates in the form 13 Jan 00UTC), and the model was allowed to run for 120 hours, i.e., until 18 Jan 00UTC. Figure 1 shows the time sequence of PV and OLR for the period of 14-17 Jan at 12UTC for the control simulation (CNTL). Comparison with NCEP reanalysis and NOAA/OLR data show that PV evolution is fairly well simulated, with high PV intrusion and deep convection occurring downstream of the intrusion (Fig. 1). This particular model setup is able to simulate convection, CAPE accumulation, vertical ascent and destabilization of the atmosphere, which are the main diagnostics we will be using to characterize or identify convection.

Numerous other simulations were performed with differing initial/boundary conditions, gridsize and physical parameterizations. Comparison between these results showed that the model is more sensitive to initial and boundary conditions (NCEP reanalysis compared to balanced fields) in predicting convection than it is to physical parameterizations or gridsize choices.

4. FACTOR SEPARATION RESULTS

We use the “factor separation method” (FSM, Stein and Alpert 1992) to evaluate the contributions of (a) the upper level PV (associated with the intrusion) and (b) latent heat, to the outgoing longwave radiation (OLR), vertical velocity, static stability (S) and convective available potential energy (CAPE).

According to the FSM, the number of simulations needed to isolate the contributions of n factors is 2^n. In the present case, $n = 2$, the factors being (a) and (b) above, and 4 simulations are required. These simulations are a control simulation with the upper level intrusion and convective processes included (run CNTL), a simulation with the upper level intrusion but the latent heat “turned off” (run UPV), the reverse of this simulation (run LH), and finally a simulation in which both upper level PV and latent heat are removed from the simulation (run OTH). The physical parameterization options were kept the same for all runs. In the runs LH and OTH the upper level PV was removed from the initial and boundary conditions. This was done in the following manner: First, a “basic state” was defined based on a 5-day mean between 13-17 Jan. Then, we select the levels in which a PV anomaly equal or greater than 1 PVU at 20°N is found for the day of southwardmost intrusion (400-100hPa for this case) and remove the PV anomaly, substituting its value by the average one. We take then this distribution, which is not in any dynamical balance, and “invert” it according to Charney’s Balance and obtain dynamically balanced fields of geopotential, wind and temperature, which are used as initial and boundary conditions for the simulations.

The bottom 3 rows of Figure 1 show the PV and OLR distributions on (a) 14 Jan 12UTC and (b) 16 Jan 12UTC for runs UPV, LH and OTH. It is clear that the convection must be related to the presence of the upper level PV anomaly, since there is no signal of OLR when intrusion is removed. This can also be seen in the thermal and vertical velocity fields, which are nearly undisturbed throughout the depth of the troposphere in both runs LH and OTH (not shown).

Figure 2a-d shows the time evolution of OLR, dry static stability S, CAPE, and vertical velocity w (= dz/dt), for the four simulations. The plots show 5x5° lat/lon area-averaged values for each of these quantities, as indicated in the top of each plot. These regions differ slightly for each variable and were chosen based on visual inspection of individual maps, such that it would include the larger area of maxima (or minima, depending on the parameter) that the box could contain.

The time sequence of OLR (Fig. 2a) for run CNTL shows that its value begin to drop substantially after 15 Jan 00UTC, reaching a deep convection threshold (~205 W.m^{-2}, e.g., Gu and Zhang 2002) at around 15 Jan 12UTC. This plot also shows that the OLR sequence from run UPV matches closely the control run until 15 Jan 12UTC, while for the remaining runs, OLR signal remains high throughout the whole simulation period. This behavior is similarly observed in the sequence of S (Fig. 23b). The variation of the static stability in the run UPV follows the curve of CNTL prior to 15 Jan 12UTC. For the other two runs, there is not decrease of S prior to this date.

Figure 2c shows that CAPE builds up prior to 15 Jan 12UTC in runs CNTL and UPV, but not in the other runs. The vertical velocity field (Fig. 2d) shows that only run UPV yields positive values of w during the PV intrusion evolution.

A question remains about the role of surface fluxes and moisture convergence in the triggering of convection. To further ascertain that the upper level PV anomaly was the crucial element to the development of convection rather than surface conditions, we show in Fig. 2e the time sequence of the latent heat flux for the same area and period of that for CAPE. It is expected that latent heat flux would be enhanced before convection is activated. We see indeed that there is an increase in the latent heat flux between 14 and 15 Jan 12UTC for run CNTL, however OTHR have the higher latent heat flux and still was unable to trigger convection. Run LH had values of latent heat flux very similar to CNTL and also failed to produce convection. These results are corroborated by the evolution of the equivalent potential temperature (θ_e) at 2m, for the same area and period (Fig. 2f). Despite the fact that (θ_e) evolution is very similar in runs CNTL and LH, the latter did not present convection, reinforcing the hypothesis that surface processes by themselves do not have a sufficient impact in triggering convection, and that the presence of the intrusion is of fundamental importance for that, at least for this case.

The factor separation method allows to quantify the contributions of each factor (upper level PV anomaly, latent heat, their interaction, and others unrelated to the previous three) to OLR, CAPE, w and S. A summary of these contributions is shown in Table1.

Apart from the tendency of S, all other parameters (OLR, CAPE and w) show that the contribution of UPV was the most important for the development of convection. For example, the total decrease of OLR from ‘clear sky’ value to control value was 67.7 W.m^{-2}. Of this, 61.1 W.m^{-2} (~90%) was due to the upper level PV only. In the case of CAPE, the upper level PV anomaly contributes with ~53% for the energy build-up for convection, and with ~61% of the upward velocity at 500hPa. The tendency of static stability shows that the decrease between 15 Jan 00-12 UTC is mostly due to LH, but there is substantial decrease in S due to UPV between 14 Jan 12UTC to 15 Jan 00UTC.

Table 1: Control values and relative contributions of upper level PV, latent heat, their interaction and factors unrelated to any of the former, for: OLR on 15 Jan 12UTC, tendency of S for the period 00-12UTC 15 Jan, average of CAPE from 12 Jan 00UTC to 15 Jan 00UTC, and vertical velocity w at 500hPa on 15 Jan 12UTC.

Factor	OLR ($W.m^{-2}$)	$\frac{\partial S_\alpha}{\partial t}\overline{[800-500hPa]}$ (10^{-5} $K.m^2.kg^{-1}.h^{-1}$)	$CAPE_\alpha$ ($J.kg^{-1}$)	w ($cm.s^{-1}$)
Area	17.5-22.5°N 215-220°E	17.5-22.5°N 210-215°E	15-20°N 207.5-212.5°E	15-20°N 210-215°E
CNTL	195.29	-0.458	428.35	3.99
UPV only	-61.14	0.609	228.84	2.44
LH only	-0.88	-1.122	75.06	-0.21
Interaction	-5.57	-0.426	-30.96	2.27
Other	262.9	0.480	95.41	-0.52

5. EFFECT OF LATENT HEAT ON INTRUSION EVOLUTION

The next step is to investigate the effect of convection – in particular, of latent heat – on PV evolution itself. Potential vorticity is conserved in adiabatic and frictionless conditions. Although those processes may be neglected in some circumstances rendering PV as a tracer, this is not true during and after the onset of convection, where turbulent mixing, latent heat release and cloud effects may cause material changes in PV. The material change of PV can be expressed as

$$\frac{DPV}{Dt}=\frac{1}{\rho}\zeta_a\cdot\nabla\dot{\theta}+\frac{1}{\rho}K\cdot\nabla\theta \qquad (1)$$

where ζ_a is the absolute vorticity, $\dot{\theta}$ is the diabatic heating term, and K is the curl of the frictional force per unit mass. The first term is the diabatic term, which include effects of radiative heating/cooling, latent heat release and heat conduction (usually neglected). The second term in the r.h.s. is the diffusive term, which usually refers to molecular dissipation (in most cases neglected) and turbulent mixing near the ground. In this study, only the impact of latent heat release on the PV evolution will be examined.

We first compare the evolution of PV in runs CNTL and UPV. Figure 1 shows snapshots of PV and OLR for these runs for two stages of evolution of the intrusion. When convection is not present yet, the two runs yield very similar PV and OLR fields. However, as the convection develops, there is a clear signal of low OLR in both runs, with difference in the position and extent of convection. Also, the intrusion is more tilted and narrow in run CNTL, as opposed to a broader and more N-S oriented high PV ridge in run UPV (16 Jan 12UTC). As the intrusion moves eastward, the low OLR distribution have a different pattern in each run, and the PV ridge is more pronounced in run CNTL. To investigate how these differences are related to latent heat and its interaction with PV evolution itself we again use the FSM. Figure 3 show the PV distribution due to the interaction of LH and PV itself (CNTL– (UPV+LH) –OTH). PV that is created or destroyed due to direct effect of latent heat covers a large area in the northern edge of the domain, however its magnitude is actually one order smaller than the actual PV (not shown). On the other hand, PV that is directly related to the interaction of PV and latent heat is more localized, and coincides with the areas of low OLR in run CNTL. The overall effect of this interaction seems to be that it sharpens the gradient of PV downstream of the ridge and causes it to be narrower too. Vertical cross section of PV and relative humidity show a similar picture: The downward penetration of PV intrusion has a shape that nearly borders the relative humidity contours at 40% when convection has developed (Fig. 4, top row (b)). In run CNTL there is PV being destroyed in the underneath and downstream of the intrusion, but in run UPV, the relative humidity field only follows the intrusion its downstream side (not shown). Figure 4 bottom row again show that the interaction of PV and latent heat produces PV of the same order of magnitude of the anomaly (but with opposite sign) coincident with the areas in the control run where PV has been ‘eaten away’.

6 SUMMARY AND CONCLUSIONS

In this work we have used the MM5 model to examine the interactions between upper level PV and convection during PV intrusions into the tropical troposphere. The model is able to simulate intrusions and convection ahead of high PV tongue. Sensitivity studies showed that the simulations are more sensitive to boundary and initial conditions than to physical parameterization choices and gridsize.

Using the factor separation method we have isolated the contributions of upper level PV anomaly associated with the intrusion, latent heat, and their interactions to address the issues proposed in the introduction. Results from MM5 simulation and FSM analysis show that the upper level PV anomaly has the dominant contribution to CAPE, static stability and vertical ascent. The interaction of latent heat and upper level PV has the next significant importance, and its contribution grows as the intrusion and convection evolves. This interaction is very important in determining the width of the PV ridge and in tightening the PV gradient downstream of the intrusion, by creating negative PV in the same order of magnitude as PV itself (i.e., O[10^0]).

The same methodology was applied to another case of deep tropical intrusion (10-16 of February 1991), which also had a PVU anomaly greater or equal to 1 at 20N between the layers 400-100 hPa. The contributions of this upper level anomaly to OLR, CAPE and vertical ascent were again dominant over the others. However, the role of the interaction of latent heat and PV on the PV is not as clear as it was in the case presented here. We are currently performing the same analysis to other intrusion cases (Waugh and Polvani, 2000) to gain further insight and to confirm the present results.

5. REFERENCES

Davis, C.A. and K.A. Emanuel, 1991: Potential vorticity diagnostics of cyclogenesis. *Mon. Wea. Rev.,* **119**, 1929-1953.

Dudhia, J., 1993: A nonhydrostatic version of the Penn State-NCAR mesoscale model: Validation tests and simulation of an Atlantic cyclone and cold front. *Mon. Wea. Rev*., **121**, 1493-1513.

Gu, G. and C. Zhang, 2002: Cloud components of the ITCZ. *J. Geophys. Res.*, 107(D21), 4565, doi:10.1029/2002JD002089.

Kiladis, G.N., 1998: Observations of Rossby waves linked to convection over the eastern tropical Pacific. *J. Atmos. Sci.*, **55**, 321-339.

______, and K.M. Weickmann, 1992: Circulation anomalies associated with tropical convection during northern winter. *Mon. Wea. Rev.*, **120**, 1900-1923.

Stein U. and P. Alpert, 1992: Factor Separation in Numerical Simulations. *J. Atmos. Sci*, **50**, 2107-2115.

Waugh, D.W. and B.M. Funatsu, 2003: Intrusions into the tropical upper troposphere: Three dimensional structure and accompanying ozone and OLR distributions. *J. Atmos. Sci.*, **60**, 637-653.

______, and L.M. Polvani, 2000: Intrusions into the tropical upper troposphere. *Geophys. Res. Lett.*, **27**, 3857-3860.

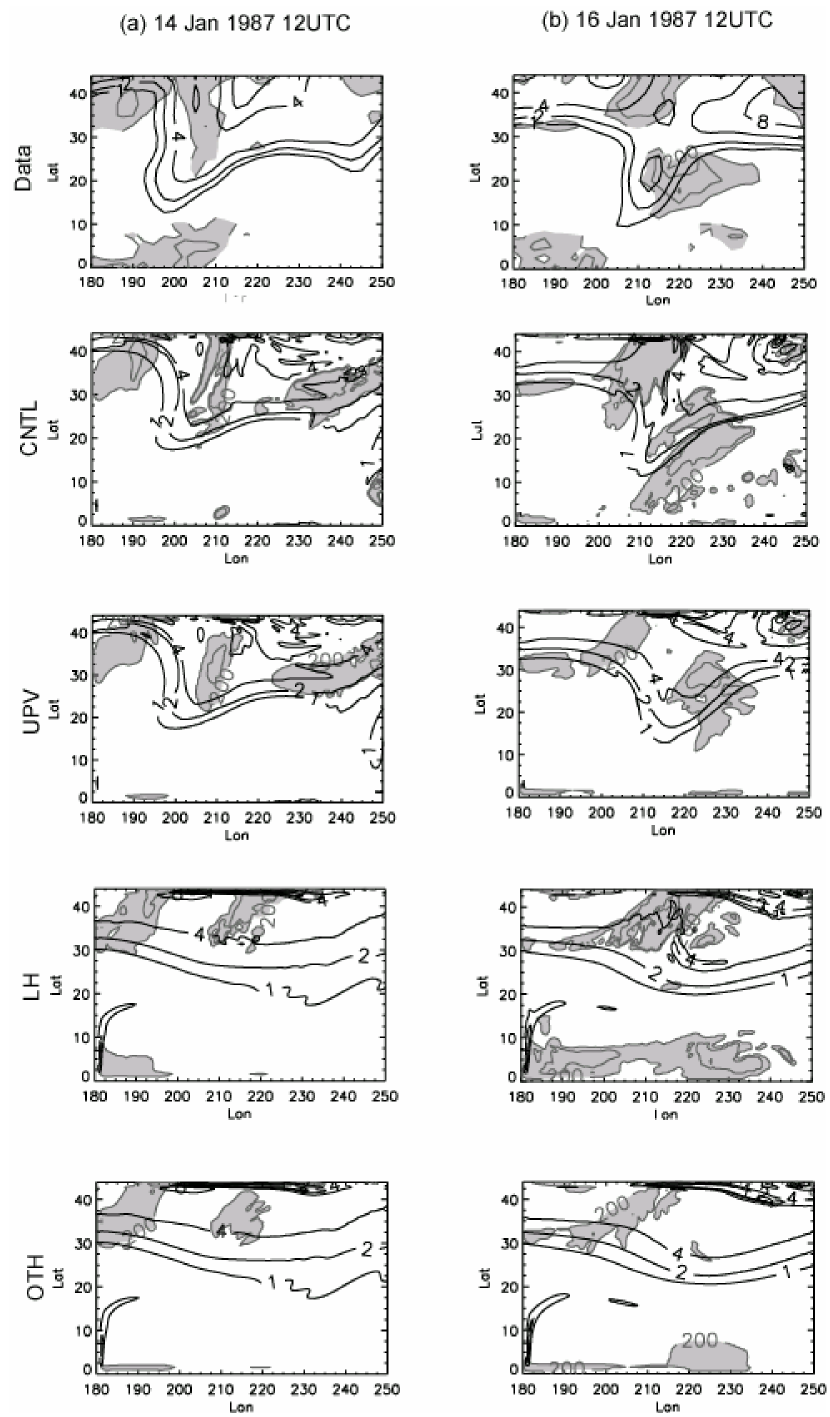

Fig. 1: Potential vorticity (1, 2, 4 and 8 PVU, 1PVU = 10^{-6} m^2 K $kg^{-1}s^{-1}$) at 200 hPA, and OLR (< 200 $W.m^{-2}$ shaded), for: (a) 14 January 1987 12UTC, and (b) 16 January 1987 12UTC, for NCEP/NOAA data (first row) and for each of the simulations indicated on the left of each row.

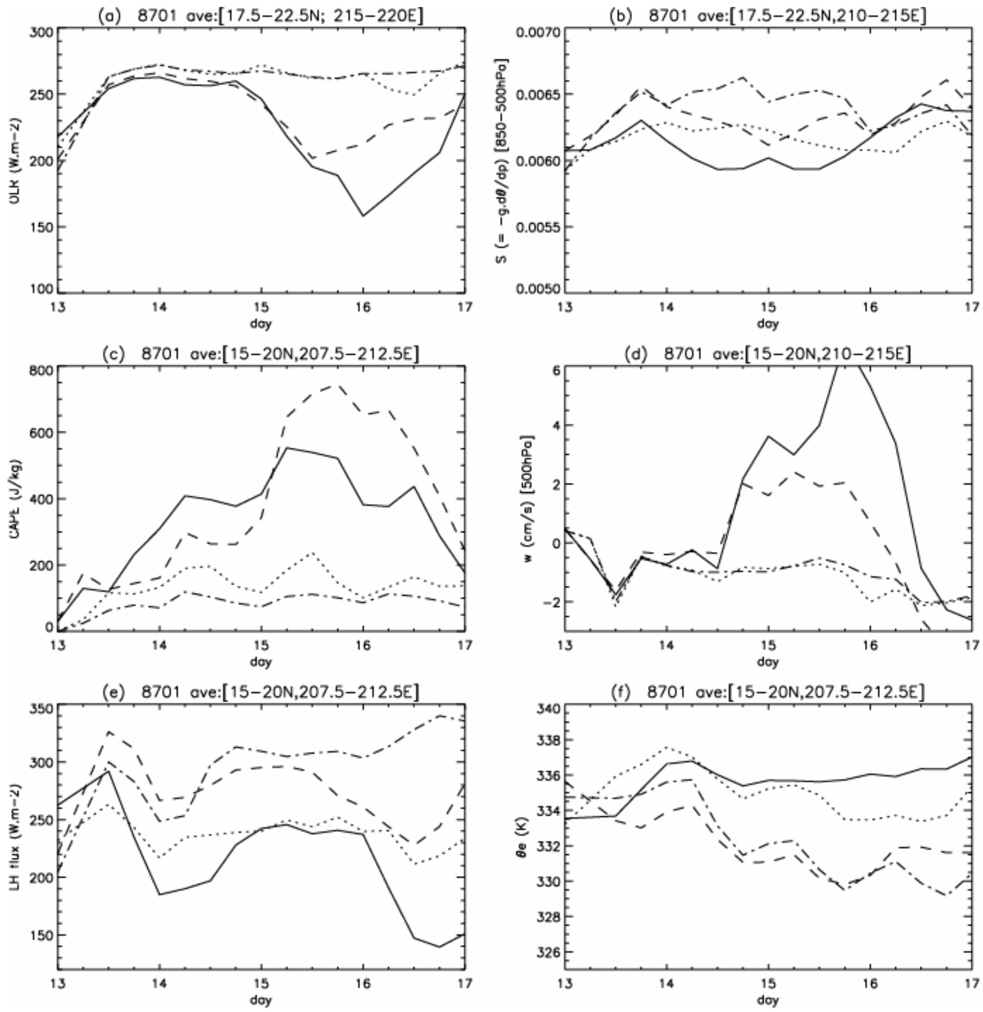

Fig. 2: Time sequence of area-averaged (a) OLR ($W.m^{-2}$), (b) dry static stability S ($K.m^2.kg^{-1}$), (c) CAPE ($J.kg^{-1}$), (d) vertical velocity w (=dz/dt), (e) latent heat flux ($W.m^{-2}$), and (f) equivalent potential temperature θ_e (K). The regions were the average was taken are shown on the top of each panel. Line style key: CNTL (including both upper level PV anomaly and latent heat) solid line, UPV (include only upper level PV anomaly) dashed line, LH (include only latent heat) dotted line, and OTH (removing both upper level PV anomaly and latent heat) dot-dashed line.

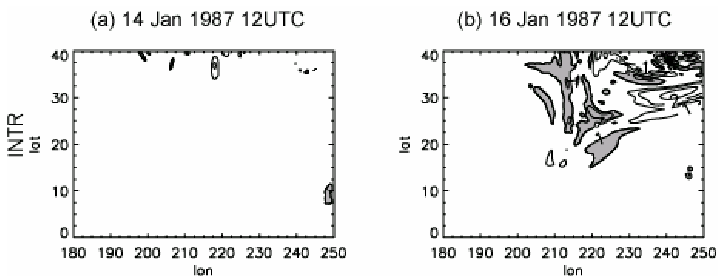

Fig. 3: Contribution of PV from the interaction of latent heat and upper level PV anomaly only at 200hPa, for the same dates as in Fig. 1. PV contours are ± 1, 2, 4 and 8 for the latter, with negative values shaded in both panels.

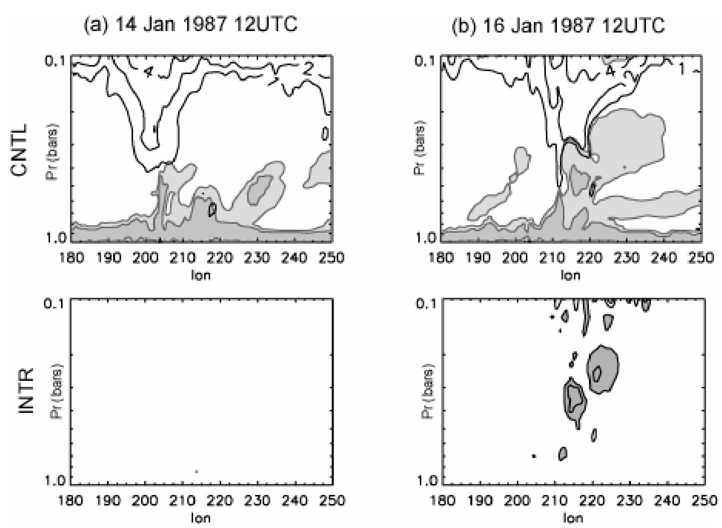

Fig. 4: Top row: Cross section of PV (solid lines, 1, 2, 4 PVU) and relative humidity (light gray: < 40%, dark gray: < 80%) at 20°N for control run. Bottom row: Contribution of PV from the interaction of latent heat and upper level PV anomaly only, at 200hPa. PV contours are ± 1, 2, 4 PVU, with negative values shaded. (a) and (b) are the same dates as in Fig. 1.